

# Separation and metrology of nanoparticles by nanofluidic size exclusion

Samuel M. Stavis,\* Jon Geist and Michael Gaitan

Received 14th May 2010, Accepted 9th July 2010

DOI: 10.1039/c0lc00029a

A nanofluidic technology for the on-chip size separation and metrology of nanoparticles is demonstrated. A nanofluidic channel was engineered with a depth profile approximated by a staircase function. Numerous stepped reductions in channel depth were used to separate a bimodal mixture of nanoparticles by nanofluidic size exclusion. Epifluorescence microscopy was used to map the size exclusion positions of individual nanoparticles to corresponding channel depths, enabling measurement of the nanoparticle size distributions and validation of the size separation mechanism.

Nanoparticle size distribution is strongly correlated with useful and harmful nanoparticle characteristics.<sup>1–4</sup> This has motivated the development of methods to purify dispersions and separate mixtures of nanoparticles of different sizes for subsequent measurement and application. Current technology for nanoparticle size processing and characterization remains a bottleneck to the fundamental understanding and safe exploitation of nanoparticles.<sup>5</sup> Conventional methods of nanoparticle size separation and purification<sup>6–14</sup> are successful but can be slow and inefficient and are typically followed by slow and specialized nanoparticle measurement techniques.<sup>15–17</sup> Microfluidic approaches to the size separation of nanoparticles promise to be fast, efficient, and integrated into total analysis systems<sup>18–22</sup> but typically remain limited to the indirect manipulation of nanoparticle ensembles and separate from methods to measure nanoparticle size. Nanofluidic devices provide the scaling advantages of microfluidic devices and enable direct control over interactions with nanoparticles at the nanometre length scale,<sup>23–27</sup> however, the vast majority of nanofluidic devices have had only a few critical dimensions.<sup>28,29</sup> This structural limitation has restricted the range and resolution of nanofluidic approaches to the manipulation and metrology of rigid nanoparticles, although nanofluidic devices have been used extensively to analyze flexible nanomaterials.<sup>30–32</sup> In this Technical note, as illustrated in Fig. 1(A), a new technology for the on-chip size separation and metrology of nanoparticles by three-dimensional (3D) nanofluidic size exclusion is demonstrated.

A nanofluidic device was fabricated using a single layer of grayscale photolithography and standard integrated circuit manufacturing tools, as described previously.<sup>29</sup> In summary, a 3D “staircase” structure with 30 steps was patterned in a thin film of photoresist on a fused silica substrate. The 3D pattern was then transferred into the substrate at the nanometre length scale by low selectivity reactive ion etching. Enclosed fluidic channels were formed by glass–glass wafer bonding.

The nanofluidic technology presented here depends on the characterization of numerous critical device dimensions. Prior to wafer bonding, the topography of the etched channel surface was mapped by scanning probe surface profilometry, as shown in

Fig. 1(B). Etch depths  $d$  were known to an uncertainty of  $<2$  nm (standard deviation). On average, the channel had a maximum depth of  $\sim 620$  nm, a minimum depth of  $\sim 80$  nm, and an average step size of  $\sim 18$  nm. A fabrication process defect resulted in a range of known step sizes from  $\sim 10$  nm to  $\sim 50$  nm, as shown in Fig. 1(B) and 2(C). The root mean square roughness of the etched channel surface was  $(2.1 \pm 0.2)$  nm (mean  $\pm$  standard deviation), as measured by atomic force microscopy. The root mean square roughness of the polished cover wafer surface was  $\leq 0.5$  nm, as specified by the manufacturer. For the nanofluidic size exclusion of rigid nanoparticles with diameters distributed from  $\sim 80$  to  $\sim 250$  nm, the channel surface roughness introduced a bias towards excluded channel depth, rather than random variation in channel depth. To account for this bias, the sum of the root mean square surface roughness values was subtracted from the average channel depth, with uncertainty in channel depth increased accordingly.

Before use, the device was filled and equilibrated with a commercial protein-based blocking solution including a high concentration of bovine serum albumin (BSA) as a primary constituent in phosphate buffered saline (PBS) at a pH of 7.2. BSA has been shown to bind to silica in a side-on mode, resulting in an adsorbed film thickness of 3 to 4 nm,<sup>33</sup> which was expected to have reduced the channel depth by 6 to 8 nm. As a result, 7 nm were subtracted from each nanofluidic channel depth, and the uncertainty in channel depth increased to a total of 2 nm (standard deviation). The roughness of the channel surfaces was assumed to have translated through a conformal coating of blocking proteins.

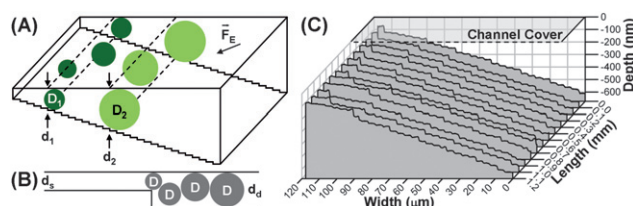


**Fig. 1** (A) Schematic of the size separation and metrology of a mixture of nanoparticles by 3D nanofluidic size exclusion. (B) Schematic of adjacent nanofluidic steps with excluded depths  $d_s < d_d$  “binning” nanoparticles of different sizes  $d_s < D < d_d$  into a size subset. Schematics are not to scale. (C) Etched channel surface as measured by scanning probe profilometry.

National Institute of Standards and Technology—Semiconductor Electronics Division, 100 Bureau Drive, Stop 8120, Gaithersburg, Maryland, 20899-8120, USA. E-mail: sstavis@nist.gov; gaitan@nist.gov; jon.geist@nist.gov; Tel: +1 (301) 975-3246

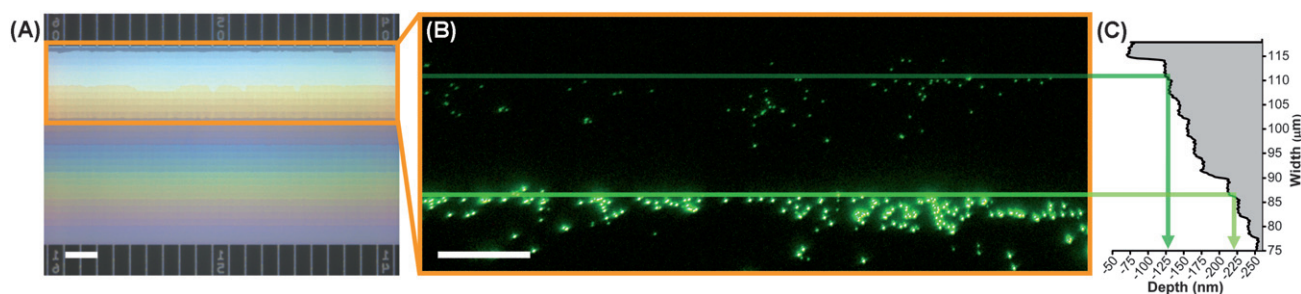


**Fig. 2** (A) Brightfield micrograph of a nanofluidic channel with thirty depths made visible by white light interference. (B) Representative epifluorescence micrograph of a mixture of polystyrene nanoparticles with bound blocking proteins and nominal diameters of  $D_1 = (112 \pm 6)$  nm and  $D_2 = (222 \pm 10)$  nm (mean  $\pm$  standard deviation) electrokinetically driven into the channel. Stepped reductions in channel depth excluded nanoparticles by size from separate regions of the channel. Primary positions of nanofluidic size exclusion are illustrated. (C) Etch depth profile of the channel region used to map positions of nanofluidic size exclusion to channel depths. Excluded channel depths were known to an uncertainty of 2 nm (standard deviation). Scale bars are 20  $\mu$ m.

Fluorescent nanoparticles were procured and prepared for nanofluidic manipulation and metrology. The structure of the nanoparticles was characterized by an amorphous polystyrene network with encapsulated fluorescent dye molecules and highly carboxylated surfaces, as specified by the manufacturer. The nanoparticles had initial diameters  $D$  of  $D_1' = (100 \pm 6)$  nm and  $D_2' = (210 \pm 10)$  nm (mean  $\pm$  standard deviation), as measured by the manufacturer using transmission electron microscopy. These values denote the first and second moments of the nanoparticle size distributions. After receipt, the nanoparticle samples were diluted to  $\sim 60$  pM, sonicated, and incubated in the same protein-based blocking solution. BSA has been shown to bind in a mixed side-on and end-on mode to carboxylated polystyrene particles similar to those used here, resulting in an adsorbed film thickness of 5 to 7 nm.<sup>34</sup> Assuming equilibrium binding, the

nanoparticle diameters were expected to have increased by 12 nm, with a negligible increase in uncertainty. As a result,  $D_1 = (112 \pm 6)$  nm and  $D_2 = (222 \pm 10)$  nm (mean  $\pm$  standard deviation) were taken as the nominal sizes of the nanoparticles with bound blocking proteins. Initial and nominal nanoparticle sizes are presented in Table 1.

The surfaces of the nanofluidic channel and nanoparticles were passivated with blocking proteins to reduce adsorption of the nanoparticles to the channel surfaces and to isolate steric hindrance of rigid nanoparticles at stepped reductions in channel depth as the mechanism for nanoparticle size separation and metrology. The resulting uncertainties in channel depths and nanoparticle sizes were propagated as described above and were small compared to the nanofluidic step sizes and nanoparticle size distribution polydispersities.

A nanoparticle size separation experiment was performed. An array of connecting channels around the central channel, visible at the top and bottom of Fig. 2(A), was used to electrokinetically drive a mixture of the two nanoparticle size distributions into the central channel. The bimodal mixture was then electrokinetically driven down the channel length and across the channel width from the deep side towards the shallow side of the staircase structure, as illustrated in Fig. 1(A). The size separation experiment was run continuously until ultimately limited by adsorption of the nanoparticles to the surfaces of the channel. Because the nanoparticles were confined to a fluidic nanostructure positioned within the depth of focus of the microscope objective, smaller and larger nanoparticles were individually visible as dimmer and brighter analytes, respectively, as shown in Fig. 2(B).

Nanofluidic size exclusion showed several advantages as a nanoparticle size separation mechanism. At the onset, sub-micrometre-scale contaminants were automatically filtered from the sample by size exclusion at the device inlet. After sample injection, Brownian motion resulted in variation in the paths taken by individual nanoparticles to stepped reductions in channel depth that resulted in nanofluidic size exclusion. This variation was irrelevant, however, because the steric hindrance of nanoparticles occurred along the staircase structure step edges independent of the preceding nanoparticle paths. Nanoparticles of different sizes reached spatially separate positions of nanofluidic size exclusion in the channel, as illustrated in Fig. 1(A) and

**Table 1** Nanoparticle sizes

Initial diameter <sup>a</sup> /nm	Nominal diameter <sup>b</sup> /nm	Measured diameter <sup>c</sup> /nm
$D_1' = (100 \pm 6)$	$D_1 = (112 \pm 6)$	$(60 \pm 2) < (12 \pm 6)\%$ $< (112 \pm 2)$ $(112 \pm 2) < (44 \pm 6)\%$ $< (119 \pm 2)$ $(119 \pm 2) < (32 \pm 6)\%$ $< (132 \pm 2)$ $(132 \pm 2) < (12 \pm 6)\%$
$D_2' = (210 \pm 10)$	$D_2 = (222 \pm 10)$	$(162 \pm 2) < (3 \pm 6)\%$ $< (201 \pm 2)$ $(201 \pm 2) < (55 \pm 6)\%$ $< (216 \pm 2)$ $(216 \pm 2) < (22 \pm 6)\%$ $< (230 \pm 2)$ $(230 \pm 2) < (12 \pm 6)\%$ $< (241 \pm 2)$ $(241 \pm 2) < (7 \pm 6)\%$

<sup>a</sup> Initial diameter: nanoparticle sizes as measured using transmission electron microscopy. <sup>b</sup> Nominal diameter: nanoparticle sizes as expected in solution with adsorbed BSA. <sup>c</sup> Measured diameter: nanoparticle size distributions as measured by mapping nanofluidic size exclusion positions of individual nanoparticles to corresponding channel depths. The percent of each size distribution separated and bounded by sequential nanofluidic steps is presented. All size values denote (mean  $\pm$  standard deviation).

as shown in Fig. 2(B). The nanoparticle mixture was separated in  $\sim 10$  seconds and within  $\sim 100$   $\mu\text{m}$  of channel width, as measured from the point of sample injection to the final nanofluidic step resulting in size exclusion. This is significantly faster and more compact than most current methods, and the separation time and distance can be further reduced by patterning narrower steps. Following nanofluidic size exclusion, the electrokinetic force tended to oppose the free diffusion of nanoparticles into deeper regions of the channel, as suggested by subsequent measurements of nanoparticle size distribution which do not show a resulting systematic overestimate of nanoparticle size. This could be exploited in the future for simultaneous nanoparticle separation and concentration.<sup>26</sup>

For the experimental results presented here, the ability to discriminate between nanoparticles of different sizes was limited primarily by the nanofluidic step size, as illustrated in Fig. 1(B). For adjacent nanofluidic steps with average excluded depths  $d_s < d_d$ , nanoparticles with different diameters  $D$  in the range of  $d_s < D < d_d$  were similarly excluded from regions of the channel with depths  $d \leq d_s$  by the edge between the nanofluidic steps. Nanoparticles in this size range were thus “binned” into a size subset by the adjacent nanofluidic steps, with smaller nanoparticle size differences unresolved.

Because the polydispersities of both nanoparticle size distributions exceeded the nanofluidic step sizes, as illustrated in Fig. 1(A), nanofluidic size exclusion enabled the separation of each nanoparticle size distribution into several discrete size subsets. For both nanoparticle size distributions, majority size subsets reached primary positions of nanofluidic size exclusion in the channel, as shown in Fig. 2. Minority size subsets reached spatially separate positions of nanofluidic size exclusion distributed around these primary positions.

Small numbers of nanoparticles were also excluded from regions of the channel that were deeper than expected. Several experimental artifacts may have contributed to a false interpretation of large nanoparticle outliers including irregular channel surface topography, adsorption of the nanoparticles to the channel surfaces, diffusion of nanoparticles away from the stepped reductions in channel depth resulting in nanofluidic size exclusion, or variation in blocking protein coverage. Alternatively, several phenomena of interest could have increased the actual sizes of these nanoparticles as characterized by nanofluidic size exclusion, such as a long tail in the size distribution or irregular nanoparticle morphology.

To measure the sizes of individual nanoparticles, positions of nanofluidic size exclusion as measured by epifluorescence microscopy were mapped to corresponding channel depths, as illustrated in Fig. 2. Nanoparticle size separation and metrology were thus integrated by this dual nanofluidic device functionality. Approximately 300 nanoparticles were analyzed for both  $D_1$  and  $D_2$ , giving sampling errors of  $<6\%$  of the measured values. The percentages of nanoparticles binned by adjacent nanofluidic steps into size subsets of the total populations and the resulting size distributions are presented in Table 1 along with initial and nominal values. Due to the artifacts discussed above, it was not possible to produce reliable upper bounds in size for the small number of large nanoparticles observed in both size distributions. As a result, only lower bounds for these size subsets are presented. Considering the measurement uncertainties, the

nanoparticle size distributions as measured by the use of the nanofluidic channel as a reference material in conjunction with nanofluidic size exclusion are in reasonable agreement with the nominal values. The smaller and larger nanoparticle size distributions are systematically over- and underestimated, respectively, indicating an uncorrected source of error that may be attributed to the possible artifacts described above. Nonetheless, these measurements of nanoparticle size distribution are sufficiently accurate for proof of concept.

These results validate the nanofluidic technology for the integrated size separation and metrology of nanoparticles demonstrated here and emphasize several of its benefits. The size separation of nanoparticles within a nanofluidic reference material provides a direct measurement mechanism and a simple model to interpret the results as well as a short traceability chain to the International System of Units (SI). The analysis of individual nanoparticles enables a full characterization of nanoparticle size distribution including moments and outliers that can be obscured by an ensemble analysis. This is an important result of this note, as dispersity in size is known to be critical in many investigations and applications of nanoparticles.<sup>5</sup> Looking forward, on-chip nanofluidic test structures have the potential to be faster and more pervasive than slow and specialized instrumentation for nanoparticle metrology.

There were several limits to the separation and metrology of nanoparticles as implemented, but none are fundamental. For the device presented here, the range of particle sizes that could be processed extended from  $\sim 80$  nm to  $\sim 620$  nm, however, the shallowest device depth can be reduced to  $<10$  nm<sup>29</sup> while the deepest device depth can be increased into the micrometre range by the use of a more selective etch. The ability to resolve nanoparticle size differences was limited primarily by the average nanofluidic step size of  $\sim 18$  nm, but step size can be reduced to  $<10$  nm by the variation of several nanofabrication process parameters, such as the use of a less selective etch or the specification of more precise photomask critical dimensions.<sup>29</sup> These range and resolution limits encompass many nanoparticle investigations and applications of current interest. The roughness of the channel surfaces ultimately limited control over channel depths, which would become increasingly problematic for smaller nanoparticles. As a result, channel surface roughness must be minimized and more accurately characterized for such samples. For the experimental results presented here, adsorption of the nanoparticles to the channel ultimately limited the ability to manipulate and measure nanoparticles. As is the case for many analytical methods involving high surface-to-volume ratio fluidic devices and analytes, surface chemistry can be limiting and must be optimized for practical applications involving specific samples of interest.

In conclusion, a nanofluidic technology for the integrated size separation and metrology of nanoparticles is presented. In a previous manuscript,<sup>29</sup> the nanofluidic size exclusion of one size of nanoparticle in a 3D nanofluidic structure was demonstrated, indicating the feasibility of the approach described here. The results presented in this note suggest that an optimized approach could be used for the on-chip sorting of nanoparticles by size and surface structure, with range and resolution designed for specific applications and determined by control over numerous nanofluidic structure depths.

## Acknowledgements

This research was performed while S.M.S. held a National Research Council Research Associateship Award at the National Institute of Standards and Technology (NIST). Device fabrication was performed at the Cornell Nanoscale Science and Technology Facility (CNF), a member of the National Nanotechnology Infrastructure Network, and the Cornell Center for Materials Research, both supported by the National Science Foundation. Device characterization was performed in part at the NIST Center for Nanoscale Science and Technology. The authors gratefully acknowledge the CNF staff for assistance with device fabrication and Brian J. Nablo and Elizabeth A. Strychalski for helpful discussions.

## Notes and references

- 1 K. K. Likharev, *Proc. IEEE*, 1999, **87**, 606–632.
- 2 X. Michalet, F. F. Pinaud, L. A. Bentolila, J. M. Tsay, S. Doose, J. J. Li, G. Sundaresan, A. M. Wu, S. S. Gambhir and S. Weiss, *Science*, 2005, **307**, 538–544.
- 3 S. M. Moghimi, A. C. Hunter and J. C. Murray, *FASEB J.*, 2005, **19**, 311–330.
- 4 A. Nel, T. Xia, L. Madler and N. Li, *Science*, 2006, **311**, 622–627.
- 5 E. K. Richman and J. E. Hutchison, *ACS Nano*, 2009, **3**, 2441–2446.
- 6 H. C. Schwarzer and W. Peukert, *Chem. Eng. Commun.*, 2004, **191**, 580–606.
- 7 K. Langer, S. Balthasar, V. Vogel, N. Dinauer, H. von Briesen and D. Schubert, *Int. J. Pharm.*, 2003, **257**, 169–180.
- 8 Q. L. Xie, J. Liu, X. X. Xu, G. B. Han, H. P. Xia and X. M. He, *Sep. Purif. Technol.*, 2009, **66**, 148–152.
- 9 J. C. Giddings, *Science*, 1993, **260**, 1456–1465.
- 10 J. P. Novak, C. Nickerson, S. Franzen and D. L. Feldheim, *Anal. Chem.*, 2001, **73**, 5758–5761.
- 11 G. T. Wei, F. K. Liu and C. R. C. Wang, *Anal. Chem.*, 1999, **71**, 2085–2091.
- 12 M. Hanauer, S. Pierrat, I. Zins, A. Lotz and C. Sonnichsen, *Nano Lett.*, 2007, **7**, 2881–2885.
- 13 F. K. Liu and G. T. Wei, *Anal. Chim. Acta*, 2004, **510**, 77–83.
- 14 S. F. Sweeney, G. H. Woehrle and J. E. Hutchison, *J. Am. Chem. Soc.*, 2006, **128**, 3190–3197.
- 15 Z. L. Wang, *J. Phys. Chem. B*, 2000, **104**, 1153–1175.
- 16 K. C. Grabar, K. R. Brown, C. D. Keating, S. J. Stranick, S. L. Tang and M. J. Natan, *Anal. Chem.*, 1997, **69**, 471–477.
- 17 F. Scheffold and P. Schurtenberger, *Soft Mater.*, 2003, **1**, 139–165.
- 18 A. L. Vig and A. Kristensen, *Appl. Phys. Lett.*, 2008, **93**, 3.
- 19 L. R. Huang, E. C. Cox, R. H. Austin and J. C. Sturm, *Science*, 2004, **304**, 987–990.
- 20 D. W. Inglis, J. A. Davis, R. H. Austin and J. C. Sturm, *Lab Chip*, 2006, **6**, 655–658.
- 21 M. Durr, J. Kentsch, T. Muller, T. Schnelle and M. Stelzle, *Electrophoresis*, 2003, **24**, 722–731.
- 22 M. L. Y. Sin, Y. Shimabukuro and P. K. Wong, *Nanotechnology*, 2009, **20**, 9.
- 23 D. Huh, K. L. Mills, X. Y. Zhu, M. A. Burns, M. D. Thouless and S. Takayama, *Nat. Mater.*, 2007, **6**, 424–428.
- 24 A. H. J. Yang, S. D. Moore, B. S. Schmidt, M. Klug, M. Lipson and D. Erickson, *Nature*, 2009, **457**, 71–75.
- 25 M. Wang, N. Jing, I. H. Chou, G. L. Cote and J. Kameoka, *Lab Chip*, 2007, **7**, 630–632.
- 26 S. M. Park, Y. S. Huh, H. G. Craighead and D. Erickson, *Proc. Natl. Acad. Sci. U. S. A.*, 2009, **106**, 15549–15554.
- 27 M. N. Hamblin, J. Xuan, D. Maynes, H. D. Tolley, D. M. Belnap, A. T. Woolley, M. L. Lee and A. R. Hawkins, *Lab Chip*, 2010, **10**, 173–178.
- 28 E. A. Strychalski, S. M. Stavis and H. G. Craighead, *Nanotechnology*, 2008, **19**, 8.
- 29 S. M. Stavis, E. A. Strychalski and M. Gaitan, *Nanotechnology*, 2009, **20**, 7.
- 30 J. Han and H. G. Craighead, *Science*, 2000, **288**, 1026–1029.
- 31 W. Reisner, K. J. Morton, R. Riehn, Y. M. Wang, Z. N. Yu, M. Rosen, J. C. Sturm, S. Y. Chou, E. Frey and R. H. Austin, *Phys. Rev. Lett.*, 2005, **94**, 196101.
- 32 C. H. Reccius, S. M. Stavis, J. T. Mannion, L. P. Walker and H. G. Craighead, *Biophys. J.*, 2008, **95**, 273–286.
- 33 T. J. Su, J. R. Lu, R. K. Thomas, Z. F. Cui and J. Penfold, *J. Phys. Chem. B*, 1998, **102**, 8100–8108.
- 34 J. Y. Yoon, H. Y. Park, J. H. Kim and W. S. Kim, *J. Colloid Interface Sci.*, 1996, **177**, 613–620.